

# Modeling the uncertainty on the covariance matrix for probabilistic forecast reconciliation

Chiara Carrara<sup>a,b,\*</sup>, Dario Azzimonti<sup>b</sup>, Giorgio Corani<sup>b</sup>, Lorenzo Zambon<sup>b</sup>

<sup>a</sup>University of Pavia

<sup>b</sup>SUPSI, Istituto Dalle Molle di Studi sull'Intelligenza Artificiale (IDSIA)

---

## Abstract

In forecast reconciliation, the covariance matrix of the base forecasts errors plays a crucial role. Typically, this matrix is estimated and then treated as known. In contrast, we propose a Bayesian reconciliation model that accounts for the uncertainty in the estimation of the covariance matrix. This leads to a reconciled predictive distribution that follows a multivariate t-distribution, obtained in closed-form, rather than a multivariate Gaussian distribution. We evaluate our method on three tourism-related datasets, including a new publicly available dataset. Empirical results show that our approach consistently improves prediction intervals compared to Gaussian reconciliation.

*Keywords:* Probabilistic forecast reconciliation, Covariance matrix uncertainty, Tourism forecasting, Bayesian modeling

---

## 1. Introduction

Hierarchical time series are collections of time series that adhere to a set of linear constraints. For example, the sales of individual items (the lower level of the hierarchy) are summed up to obtain the sales of different categories or stores (the upper levels of the hierarchy). Forecasts for hierarchical time series need to be *coherent*, meaning that the lower-level forecasts sum to the forecasts of the higher levels. However, the *base forecasts*, which are independently produced for each time series, are generally incoherent. *Forecast reconciliation* adjusts the base forecasts to produce coherent forecasts for the entire hierarchy.

While early works focused on the reconciliation of the point forecasts (Hyndman, Ahmed, Athanasopoulos & Shang, 2011; Wickramasuriya, Athanasopoulos & Hyndman, 2019), the most recent literature deals with *probabilistic reconciliation* (Corani, Azzimonti, Augusto & Zaffalon, 2020; Panagiotelis, Gamakumara, Athanasopoulos & Hyndman, 2023; Wickramasuriya, 2024), which quantifies the uncertainty of the reconciled predictions. The covariance matrix of the base forecast errors plays a crucial role, as it significantly impacts the performance of both reconciled point forecasts (Panagiotelis, Athanasopoulos, Gamakumara & Hyndman, 2021) and distributions (Girolimetto, Athanasopoulos, Di Fonzo & Hyndman, 2024).

The MinT reconciliation method is provably optimal with respect to both the expected mean squared error of the point forecasts (Wickramasuriya et al., 2019) and the logarithmic score (Wickramasuriya, 2024) of the reconciled distribution. However, this optimality holds only under the fundamental assumption that the covariance matrix is known.

In practice the covariance matrix is estimated from in-sample residuals. Since the number of estimated parameters grows quadratically with the number of time series, the uncertainty associated with this estimation can be substantial. If the covariance matrix is assumed to be known, this uncertainty is ignored and the uncertainty of the reconciled forecasts is underestimated (Pritularga, Svetunkov & Kourentzes, 2021).

Indeed, reconciled predictive distributions frequently suffer from *undercoverage*. The base forecasts often exhibit undercoverage of the prediction intervals (Athanasopoulos, Hyndman, Song & Wu, 2011); moreover, the variance of the predictive distribution systematically decreases after MinT reconciliation (Zambon, Agosto,

---

\*Corresponding author

*Email addresses:* chiara.carrara03@universitadipavia.it (Chiara Carrara), dario.azzimonti@supsi.ch (Dario Azzimonti), giorgio.corani@supsi.ch (Giorgio Corani), lorenzo.zambon@supsi.ch (Lorenzo Zambon)

Giudici & Corani, 2024a). If the covariance matrix is known, this reduction is optimal; but if the estimation of the covariance matrix is uncertain, this can lead to undercoverage of the reconciled prediction intervals. Recent works combine reconciliation with conformal prediction so that the prediction intervals (PI) achieve nominal coverage (Principato, Stoltz, Amara-Ouali, Goude, Hamrouche & Poggi, 2025). However, to date, no reconciliation framework accounts for the uncertainty of the covariance matrix.

In this paper, we propose a Bayesian reconciliation approach that models the uncertainty of the covariance matrix. By adopting a Bayesian framework, we integrate parameter uncertainty into the predictive distribution (Gelman, Carlin, Stern, Dunson, Vehtari & Rubin, 2013, Chap. 1.3), yielding a more principled quantification of the uncertainty. We assume an Inverse-Wishart (IW) prior distribution for the covariance matrix  $\mathbf{W}$  and we update it using the in-sample residuals, which we assume to be jointly Gaussian, conditionally on  $\mathbf{W}$ . From the resulting posterior, we analytically derive the incoherent posterior predictive distribution, which is a multivariate  $t$ . We then apply reconciliation via conditioning (Corani et al., 2020; Zambon, Azzimonti & Corani, 2024b). Crucially, we obtain the reconciled distribution in closed-form, thanks to the closure properties of the multivariate  $t$ . This represents the only known analytical solution for reconciliation via conditioning besides the Gaussian case (Zambon et al., 2024a). The resulting coherent reconciled distribution is a multivariate  $t$ ; we thus call our method *t-Rec*.

We analyze a minimal hierarchy to gain theoretical insights into the properties of the reconciled distribution. Unlike the Gaussian case, the reconciled variance depends on the incoherence of the base forecasts, allowing for prediction intervals to widen; we confirm this behavior via simulations. We also empirically show that, as the training length grows, the effect of modeling the covariance uncertainty vanishes.

Finally, we evaluate our method on three distinct datasets, including a novel dataset on Swiss tourism. In all settings, *t-Rec* yields point forecasts comparable to state-of-the-art Gaussian reconciliation (Wickramasuriya, 2024; Zambon et al., 2024b) but consistently improves the probabilistic forecasts.

The paper is structured as follows: in Sect. 2 we introduce the notation and recall the concepts of probabilistic reconciliation; in Sect. 3 we analytically derive *t-Rec* and discuss its specifications; in Sect. 4 we demonstrate the model’s behavior on a minimal hierarchy; in Sect. 5 we report empirical results on real datasets; in Sect. 6 we present our conclusions.

## 2. Probabilistic reconciliation

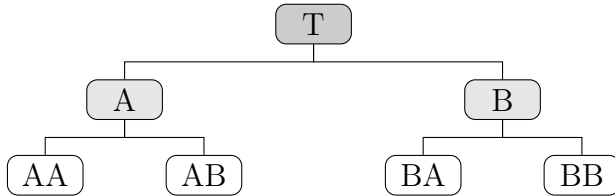


Figure 1: Hierarchy with 4 bottom and 3 upper time series.

Fig. 1 is an example of hierarchical time series, which can, for instance, represent the total visitors of a country (T), disaggregated by zones (A, B) and regions (AA, AB, BA, BB), so that:

$$T = A + B, \quad A = AA + AB, \quad B = BA + BB.$$

At any time  $t$ , the hierarchical constraints between time series are given by:

$$\mathbf{u}_t = \mathbf{A}\mathbf{b}_t, \tag{1}$$

where  $\mathbf{A} \in \mathbb{R}^{n_u \times n_b}$  is the *aggregation matrix*, which is made of 0 and 1 and specifies how the *bottom* time series  $\mathbf{b}_t \in \mathbb{R}^{n_b}$  aggregate to the *upper* time series  $\mathbf{u}_t \in \mathbb{R}^{n_u}$ . Denoting  $\mathbf{y}_t = [\mathbf{u}_t^T, \mathbf{b}_t^T]^T \in \mathbb{R}^n$ , we can equivalently encode the hierarchy as  $\mathbf{y}_t = \mathbf{S}\mathbf{b}_t$ , where the *summing matrix*  $\mathbf{S} \in \mathbb{R}^{n \times n_b}$  is:

$$\mathbf{S} = \begin{bmatrix} \mathbf{A} \\ \mathbf{I}_{n_b \times n_b} \end{bmatrix}.$$

Girolimetto & Di Fonzo (2024) introduce a more general framework for linearly constrained time series that does not rely on the summing matrix. Our method is applicable also to that case; however, in the following, we adopt the standard setting based on  $\mathbf{S}$ .

We consider probabilistic forecasts in the form of a joint predictive distribution  $\hat{\pi}$  over  $\mathbb{R}^n$ . A forecast distribution is *coherent* if it gives positive probability only to regions of points that satisfy the hierarchical constraints. Thus the support of a coherent distribution lies on the *coherent subspace*  $\mathcal{S}$ , defined as  $\mathcal{S} := \{\mathbf{y} \in \mathbb{R}^n \text{ such that } \mathbf{y} = \mathbf{S}\mathbf{b}\}$ . Probabilistic reconciliation (Panagiotelis et al., 2023; Zambon et al., 2024b) adjusts the initially incoherent base forecast distribution  $\hat{\pi}$  to obtain a coherent reconciled forecast distribution  $\tilde{\pi}$ .

*MinT reconciliation.* The Minimum Trace (MinT) reconciliation method was introduced for the reconciliation of point forecasts (Wickramasuriya et al., 2019). Given the  $h$ -step ahead base point forecasts  $\hat{\mathbf{y}}_{t+h|t}$ , computed at time  $t$  for time  $t+h$ , the reconciled point forecasts  $\tilde{\mathbf{y}}_{t+h|t}$  are obtained by projecting  $\hat{\mathbf{y}}_{t+h|t}$  on the coherent subspace  $\mathcal{S}$ :

$$\tilde{\mathbf{y}}_{t+h|t} = \mathbf{S}\mathbf{P}_h\hat{\mathbf{y}}_{t+h|t}, \quad (2)$$

where  $\mathbf{P}_h = (\mathbf{S}^T\mathbf{W}_h^{-1}\mathbf{S})^{-1}\mathbf{S}^T\mathbf{W}_h^{-1}$ , and  $\mathbf{W}_h$  is the covariance matrix of the  $h$ -step ahead base forecast errors. Assuming that the base forecasts  $\hat{\mathbf{y}}_{t+h|t}$  are unbiased and that  $\mathbf{W}_h$  is known, the reconciled point forecasts  $\tilde{\mathbf{y}}_{t+h|t}$  minimize the expected mean squared error (MSE).

MinT was later extended to the probabilistic case by projecting on  $\mathcal{S}$  the entire forecast distribution  $\hat{\pi}$  (Panagiotelis et al., 2023). If the joint base forecast distribution is Gaussian, i.e.,  $\hat{\pi} = \mathcal{N}(\hat{\mathbf{y}}_{t+h|t}, \mathbf{W}_h)$ , the reconciled distribution is also Gaussian:

$$\tilde{\pi} = \mathcal{N}(\tilde{\mathbf{y}}_{t+h|t}, \tilde{\mathbf{W}}_h),$$

where  $\tilde{\mathbf{y}}_{t+h|t}$  is given by Eq. (2) and  $\tilde{\mathbf{W}}_h = \mathbf{S}\mathbf{P}_h\mathbf{W}_h\mathbf{P}_h^T\mathbf{S}^T$ . In this case,  $\tilde{\pi}$  is optimal with respect to the log-score (Wickramasuriya, 2024).

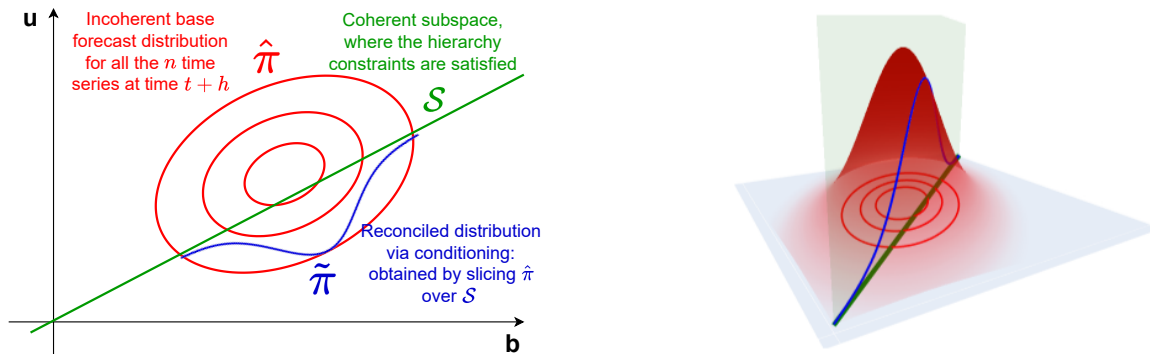


Figure 2: Reconciliation via conditioning: the reconciled distribution  $\tilde{\pi}$  is obtained by slicing  $\hat{\pi}$  on the coherent subspace  $\mathcal{S}$ .

*Probabilistic reconciliation via conditioning.* An alternative approach to probabilistic reconciliation derives the reconciled distribution by conditioning the joint base forecast distribution on the hierarchical constraints (Corani et al., 2020; Zambon et al., 2024b). Given  $\hat{\mathbf{Y}}_{t+h|t} = [\hat{\mathbf{U}}_{t+h|t}^T, \hat{\mathbf{B}}_{t+h|t}^T]^T$ , a random vector distributed as the  $h$ -step ahead base forecast distribution  $\hat{\pi}$ , the reconciled distribution of the bottom series is specified by

$$\tilde{\mathbf{B}}_{t+h|t} \sim \hat{\mathbf{B}}_{t+h|t} \mid (\hat{\mathbf{U}}_{t+h|t} - \mathbf{A}\hat{\mathbf{B}}_{t+h|t} = 0), \quad (3)$$

and it can be extended to the entire hierarchy via

$$\tilde{\mathbf{Y}}_{t+h|t} = \mathbf{S}\tilde{\mathbf{B}}_{t+h|t}. \quad (4)$$

Eq. (3) allows the computation of the reconciled density up to a normalizing constant. Generally, the reconciled distribution is not available in closed form, thus requiring sampling approaches (Corani, Azzimonti & Rubattu, 2024; Zambon et al., 2024b). To date, the only exception is when the base forecast distribution

is jointly Gaussian; in this case, reconciliation via conditioning can be solved analytically and coincides with MinT (Zambon et al., 2024a). Reconciliation via conditioning can be interpreted as slicing the incoherent joint density over the coherent subspace  $\mathcal{S}$  (Fig. 2).

*Estimation of  $\mathbf{W}_1$ .* For  $h = 1$ ,  $\mathbf{W}_1$  is estimated as the covariance matrix of the in-sample residuals, usually (Wickramasuriya et al., 2019; Panagiotelis et al., 2021; Di Fonzo & Girolimetto, 2024) adopting the shrinkage estimator (Schäfer & Strimmer, 2005):

$$\widehat{\mathbf{W}}_1 = (1 - \lambda_{\text{shrink}})\widehat{\mathbf{S}}_1 + \lambda_{\text{shrink}}\widehat{\mathbf{D}}_1, \quad (5)$$

where  $\widehat{\mathbf{S}}_1$  is the sample covariance matrix of the 1-step ahead residuals,  $\widehat{\mathbf{D}}_1$  is the diagonal matrix of the sample variances, and  $\lambda_{\text{shrink}} \in [0, 1]$  is the shrinkage parameter. In what follows, we denote by *MinT* the MinT reconciliation method with the shrinkage estimator  $\widehat{\mathbf{W}}_1$ . Double shrinkage approaches (Wickramasuriya, 2017, Chap. 4.3.3; Carrara, Zambon, Azzimonti & Corani, 2025) shrink  $\widehat{\mathbf{S}}_1$  towards two targets simultaneously; however only provide limited improvements over traditional shrinkage or incur in significant computational cost.

*Estimation of  $\mathbf{W}_h$ .* There is no standard method for estimating  $\mathbf{W}_h$  for  $h > 1$ . Wickramasuriya et al. (2019) assume  $\mathbf{W}_h = k_h \mathbf{W}_1$  for some constant  $k_h$ , which can be left unspecified for computing the reconciled point forecasts. Some heuristics for setting  $k_h$  in the probabilistic framework have been proposed by Corani et al. (2020). Girolimetto et al. (2024) takes instead a different approach, estimating  $\mathbf{W}_h$  using multi-step residuals. While our method can be applied with any choice of  $\mathbf{W}_h$ , in our experiments, for simplicity, we only consider  $h = 1$ . In the following, we drop the  $h$  subscript for ease of notation.

### 3. Probabilistic reconciliation modeling the uncertainty on $\mathbf{W}$

We propose a Bayesian approach which treats  $\mathbf{W}$  as a random variable, rather than as a fixed matrix. We set a prior distribution on  $\mathbf{W}$  and update it using the information from the in-sample residuals. We account for the uncertainty on  $\mathbf{W}$  by modeling its entire posterior distribution, rather than taking a point estimate  $\widehat{\mathbf{W}}$  as in previous works. By adopting an Inverse-Wishart prior and assuming Gaussian residuals, the resulting incoherent predictive distribution is a multivariate t. We reconcile it via conditioning, obtaining a coherent multivariate t in closed-form. This is thus the second known case of closed-form reconciliation via conditioning, besides the Gaussian one. We call our method *t-Rec*.

*Prior of  $\mathbf{W}$ .* We adopt an Inverse-Wishart (IW) prior distribution for  $\mathbf{W}$ :

$$\mathbf{W} \sim \text{IW}(\boldsymbol{\Psi}_0, \nu_0). \quad (6)$$

The Inverse-Wishart is a distribution defined on the space of positive-definite matrices (Gupta & Nagar, 2018);  $\nu_0 \in \mathbb{R}$  is the degree of freedom and  $\boldsymbol{\Psi}_0 \in \mathbb{R}^{n \times n}$  is the scale matrix, which is proportional to the mean.

*Likelihood of the residuals.* We assume that the in-sample residuals  $\mathbf{r}_1, \dots, \mathbf{r}_T$ , defined as  $\mathbf{r}_j = \widehat{\mathbf{y}}_j - \mathbf{y}_j$  for  $j = 1, \dots, T$ , are independent and identically distributed (IID). This is a tenable assumption if the base forecasts are generated comparing a wide set of competing models (Svetunkov, 2023, Chap. 1.4.1; Hyndman & Athanasopoulos, 2021, Chap. 5.4) via statistical model selection. Moreover, as in Corani et al. (2020); Wickramasuriya (2024), we assume that, conditionally on  $\mathbf{W}$ , the residuals are distributed as a multivariate Gaussian with zero mean and covariance matrix  $\mathbf{W}$ :

$$\mathbf{r}_1, \dots, \mathbf{r}_T \mid \mathbf{W} \stackrel{\text{IID}}{\sim} \mathcal{N}(\mathbf{0}, \mathbf{W}). \quad (7)$$

*Posterior of  $\mathbf{W}$ .* Given the in-sample residuals  $\mathbf{R} = [\mathbf{r}_1 \ \dots \ \mathbf{r}_T]$ , we compute the posterior distribution of  $\mathbf{W}$  via Bayes' rule (Gelman et al., 2013, Chap. 1.3):

$$\pi(\mathbf{W} | \mathbf{R}) = \frac{\pi(\mathbf{W}) \pi(\mathbf{R} | \mathbf{W})}{\pi(\mathbf{R})}.$$

Generally, in Bayesian models, the posterior distribution is not available in a closed parametric form, thus requiring sampling techniques (e.g., MCMC). However, since the Inverse-Wishart prior distribution is conjugate to the Gaussian likelihood (Gelman et al., 2013, Chap. 3.6), the posterior distribution remains Inverse-Wishart and can be computed analytically:

$$\mathbf{W} | \mathbf{R} \sim \text{IW}(\mathbf{W}; \Psi', \nu'), \quad (8)$$

with parameters  $\nu' = \nu_0 + T$  and  $\Psi' = \Psi_0 + \mathbf{R}\mathbf{R}^T \in \mathbb{R}^{n \times n}$ .

*Multivariate  $t$  incoherent predictive distribution.* From Eq. (7) follows that, given  $\mathbf{W}$ , the conditional predictive distribution  $\hat{\pi}(\mathbf{y} | \mathbf{W})$  is Gaussian. To obtain the posterior predictive distribution  $\hat{\pi}(\mathbf{y} | \mathbf{R})$ , we compute the posterior joint distribution  $\hat{\pi}(\mathbf{y}, \mathbf{W} | \mathbf{R})$  and then we marginalize out  $\mathbf{W}$ ; this yields a multivariate  $t$ -distribution (Gelman et al., 2013, Chap. 3.6):

$$\begin{aligned} \hat{\pi}(\mathbf{y} | \mathbf{R}) &= \int \hat{\pi}(\mathbf{y}, \mathbf{W} | \mathbf{R}) d\mathbf{W} \\ &= \int \hat{\pi}(\mathbf{y} | \mathbf{W}) \pi(\mathbf{W} | \mathbf{R}) d\mathbf{W} \\ &= \int \mathcal{N}(\mathbf{y}; \hat{\mathbf{y}}, \mathbf{W}) \text{IW}(\mathbf{W}; \Psi', \nu') d\mathbf{W} \\ &= \text{mt}\left(\mathbf{y}; \hat{\mathbf{y}}, \frac{1}{\nu' - n + 1} \Psi', \nu' - n + 1\right). \end{aligned} \quad (9)$$

*Reconciliation.* From Eq. (9), the incoherent posterior predictive distribution is a multivariate  $t$ -distribution:

$$[\hat{\mathbf{U}}^T, \hat{\mathbf{B}}^T]^T \sim \text{mt}\left(\hat{\mathbf{y}}, \frac{1}{\nu' - n + 1} \Psi', \nu' - n + 1\right),$$

where  $\hat{\mathbf{y}} = [\hat{\mathbf{u}}^T, \hat{\mathbf{b}}^T]^T$ , with  $\hat{\mathbf{u}} \in \mathbb{R}^{n_u}$  and  $\hat{\mathbf{b}} \in \mathbb{R}^{n_b}$ , and  $\Psi'$  can be decomposed block-by-block into  $\Psi'_U \in \mathbb{R}^{n_u \times n_u}$ ,  $\Psi'_B \in \mathbb{R}^{n_b \times n_b}$ ,  $\Psi'_{UB} \in \mathbb{R}^{n_u \times n_b}$ . In the following theorem, we provide the closed-form expression of the distribution reconciled via conditioning, i.e.,  $\tilde{\mathbf{B}} \sim \hat{\mathbf{B}} | (\hat{\mathbf{U}} - \mathbf{A}\hat{\mathbf{B}} = 0)$ . The proof, reported in Appendix A, exploits the closure of the multivariate  $t$ -distribution under affine transformations (Kotz & Nadarajah, 2004) and conditioning (Ding, 2016).

**Theorem 1.** *Under the previous assumptions on prior (Eq. (6)) and likelihood (Eq. (7)), the reconciled distribution via conditioning of the bottom time series is a multivariate  $t$ -distribution:*

$$\tilde{\mathbf{B}} \sim \text{mt}\left(\tilde{\mathbf{b}}, \tilde{\Sigma}_B, \tilde{\nu}\right), \quad (10)$$

where

$$\tilde{\mathbf{b}} = \hat{\mathbf{b}} + \left(\Psi'_{UB}{}^T - \Psi'_B \mathbf{A}^T\right) \mathbf{Q}^{-1}(\mathbf{A}\hat{\mathbf{b}} - \hat{\mathbf{u}}), \quad (11)$$

$$\tilde{\Sigma}_B = C \left[ \Psi'_B - \left(\Psi'_{UB}{}^T - \Psi'_B \mathbf{A}^T\right) \mathbf{Q}^{-1} \left(\Psi'_{UB}{}^T - \Psi'_B \mathbf{A}^T\right)^T \right], \quad (12)$$

$$\tilde{\nu} = \nu' - n_b + 1, \quad (13)$$

and

$$\begin{aligned} C &= \frac{1 + (\mathbf{A}\hat{\mathbf{b}} - \hat{\mathbf{u}})^T \mathbf{Q}^{-1} (\mathbf{A}\hat{\mathbf{b}} - \hat{\mathbf{u}})}{\tilde{\nu}}, \\ \mathbf{Q} &= \Psi'_U - \Psi'_{UB} \mathbf{A}^T - \mathbf{A} \Psi'_{UB}{}^T + \mathbf{A} \Psi'_B \mathbf{A}^T. \end{aligned}$$

Theorem 1 provides the reconciled distribution for the bottom-level time series. From Eq. (4), the reconciled distribution for the entire hierarchy is a multivariate t with mean  $\tilde{\mathbf{y}} = \mathbf{S}\tilde{\mathbf{b}}$ , scale matrix  $\mathbf{S}\tilde{\Sigma}_B\mathbf{S}^T$ , and degrees of freedom  $\tilde{\nu}$ .

### 3.1. Parameters of the prior distribution

We now discuss our choices for the scale matrix  $\Psi_0$  and the degree of freedom  $\nu_0$  of the Inverse-Wishart prior.

*Scale matrix.*  $\Psi_0 \in \mathbb{R}^{n \times n}$  is a positive definite matrix, proportional to the prior mean  $\Psi$  of the IW distribution via  $\Psi_0 = (\nu_0 - n - 1)\Psi$ . To set  $\Psi$ , we look at the covariance of the residuals of two simple methods (Hyndman & Athanasopoulos, 2021, Ch. 5.2): the naive and seasonal naive. The naive method forecasts all future values as equal to the last observation, while the seasonal naive method sets each forecast equal to the last observed value of the same season (e.g., for a monthly time series, the forecast for all future February is the last observed February value). For each time series we perform model selection between naive and seasonal naive method using the KPSS seasonality test (Hyndman & Athanasopoulos, 2021, Ch. 9.1). We set  $\Psi$  as the covariance matrix of the residuals of such simple methods, estimated using the shrinkage estimator (Schäfer & Strimmer, 2005) as in *MinT*.

*Degree of freedom.* The parameter  $\nu_0$  controls the strength of the prior: a higher value indicates stronger confidence in the prior. We set  $\nu_0 \in \mathbb{R}$  by maximizing the out-of-sample log-score, estimated via Bayesian leave-one-out (LOO) cross-validation (Vehtari, Gelman & Gabry, 2017):

$$\begin{aligned} \nu_0 &:= \arg \max_{\nu \in [n+2, 5n]} \log \left( \prod_{i=1}^T \pi(\mathbf{r}_i | \mathbf{R}_{-i}) \right) \\ &= \arg \max_{\nu \in [n+2, 5n]} \sum_{i=1}^T \log \left( \text{mt} \left( \mathbf{r}_i; 0, \frac{1}{\nu + T - n} (\Psi_0 + \mathbf{R}_{-i}\mathbf{R}_{-i}^T), \nu + T - n \right) \right), \end{aligned} \quad (14)$$

where  $\mathbf{R}_{-i} \in \mathbb{R}^{n \times (T-1)}$  is the matrix of the in-sample residuals without the column  $\mathbf{r}_i$ , and  $\pi(\mathbf{r}_i | \mathbf{R}_{-i})$  is the posterior predictive density of the residuals  $\mathbf{r}_i$ , given the observations  $\mathbf{R}_{-i}$ ; the derivation of Eq. (14) is analogous to that of Eq. (9). The LOO approach is tenable for model selection in time series (Bergmeir, Hyndman & Koo, 2018) if the residuals  $\mathbf{r}_1, \dots, \mathbf{r}_T$  are approximately IID. We restrict the search for the optimal value of  $\nu_0$  to the interval  $[n + 2, 5n]$ . Indeed, the expected value of the IW prior is not defined for  $\nu_0 < n + 2$ ; on the other hand, the optimal  $\nu_0$  has been consistently below the upper bound  $\nu_0 = 5n$ .

A naive evaluation of the objective function in Eq. (14) is computationally expensive, as it requires inverting  $T$  matrices  $\Psi_0 + \mathbf{R}_{-i}\mathbf{R}_{-i}^T$ , for  $i = 1, \dots, T$ . However, we achieve a significant speed-up by noting that these matrices are rank-1 updates of the same matrix:  $\Psi_0 + \mathbf{R}_{-i}\mathbf{R}_{-i}^T = \Psi_0 + \mathbf{R}\mathbf{R}^T - \mathbf{r}_i\mathbf{r}_i^T$ . We thus use the Sherman-Morrison formula (Sherman & Morrison, 1950) to obtain

$$(\Psi_0 + \mathbf{R}_{-i}\mathbf{R}_{-i}^T)^{-1} = (\Psi_0 + \mathbf{R}\mathbf{R}^T)^{-1} + \frac{(\Psi_0 + \mathbf{R}\mathbf{R}^T)^{-1} \mathbf{r}_i\mathbf{r}_i^T (\Psi_0 + \mathbf{R}\mathbf{R}^T)^{-1}}{1 - \mathbf{r}_i^T (\Psi_0 + \mathbf{R}\mathbf{R}^T)^{-1} \mathbf{r}_i}.$$

This requires computing only *once* the inverse of  $\Psi_0 + \mathbf{R}\mathbf{R}^T$ . We optimize  $\nu$  using the `nloptr` R package (Johnson, 2008). Even in our largest experiment ( $n = 111$ ,  $T = 60$ ), the optimization requires less than 0.5 s on a standard laptop.

## 4. Reconciliation of a minimal hierarchy

We compare *t-Rec* and *MinT* on the minimal hierarchy of Fig. 3, for which the formulas of the reconciled distributions are easier to interpret. Let  $\Psi'$  be the scale matrix of the IW posterior distribution, specified by Eq. (8), and let  $\widehat{\mathbf{W}}$  be the estimated covariance matrix used by *MinT*. For simplicity, we focus here on the

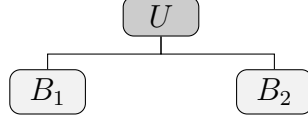


Figure 3: Hierarchy with one upper and two bottom time series.

upper series, though analogous conclusions apply to the bottom series. The reconciled marginal distributions for *MinT* (Gaussian) and *t-Rec* (univariate  $t$ ) are characterized by the following mean and scale parameters:

$$\tilde{u}^{(MinT)} = \left(1 - \frac{\hat{g}_u}{\hat{Q}}\right) \hat{u} + \frac{\hat{g}_u}{\hat{Q}} (\hat{b}_1 + \hat{b}_2), \quad \tilde{\sigma}_u^{(MinT)} = \sqrt{\hat{W}_u - \frac{\hat{g}_u^2}{\hat{Q}}}, \quad (15)$$

$$\tilde{u}^{(t-Rec)} = \left(1 - \frac{g'_u}{Q'}\right) \hat{u} + \frac{g'_u}{Q'} (\hat{b}_1 + \hat{b}_2), \quad \tilde{\sigma}_u^{(t-Rec)} = \sqrt{C \left(\Psi'_u - \frac{g'^2_u}{Q'}\right)}, \quad (16)$$

where  $g'_u$  and  $Q'$  are scalar terms derived from  $\Psi'$ , while  $\hat{g}_u$  and  $\hat{Q}$  are analogously derived from  $\widehat{\mathbf{W}}$ ; we denote by  $\Psi'_u \in \mathbb{R}$  and  $\widehat{W}_u \in \mathbb{R}$  the entries of  $\Psi'$  and  $\widehat{\mathbf{W}}$  corresponding to the upper series. We report the complete expression of the reconciled distribution for *t-Rec* in Appendix A.1, while for *MinT* we refer to Zambon et al. (2024a).

Both for *MinT* and *t-Rec*, the reconciled mean  $\tilde{u}$  is a convex combination of  $\hat{u}$  and  $\hat{b}_1 + \hat{b}_2$ . However, there is an important difference in the prediction intervals. After *MinT* reconciliation, the width of the prediction interval always decreases, as the reconciled variance is smaller than the variance of the base forecasts (Zambon et al., 2024a). In contrast, the prediction intervals of *t-Rec* can be wider than those of the base forecasts, since the  $t$  distribution has generally heavier tails than the Gaussian. Moreover, the scale of the reconciled distribution is proportional to the square root of the factor

$$C = \frac{1}{\hat{\nu}} \left(1 + \frac{(\hat{u} - \hat{b}_1 - \hat{b}_2)^2}{Q'}\right),$$

where  $\hat{u} - \hat{b}_1 - \hat{b}_2$  and  $Q'$  are respectively the mean and the variance of the random variable  $\widehat{\mathbf{U}} - \widehat{\mathbf{B}}_1 - \widehat{\mathbf{B}}_2$ , which represents the incoherence. A large *scaled incoherence*, defined as  $|\hat{u} - \hat{b}_1 - \hat{b}_2| / Q'^{1/2}$ , increases the value of  $C$ , and thus the scale of the reconciled distribution. Hence, unlike *MinT*, *t-Rec* widens the prediction intervals when faced with high incoherence, reflecting an increased uncertainty.

#### 4.1. Simulations

We perform a simulation study in which we generate time series, compute the Gaussian base forecasts and reconcile them with *MinT* and *t-Rec*. We consider the minimal hierarchy in Fig. 3 and, as in Wickramasuriya et al. (2019), we simulate the two bottom series as a structural time series model with trend, seasonality (which is set to 4), and correlated errors. We obtain the upper series as the sum of the bottom series. See Appendix B for more details on the data generating process. The base forecasts are purposely misspecified as we compute them using ets with additive noise from the R package `forecast` (Hyndman & Khandakar, 2008). We introduce the *relative width* of the prediction intervals (PI) as:

$$\text{relative width} = \frac{\text{width of the reconciled PI}}{\text{width of the base forecast PI}}.$$

In Fig. 4, we show the distribution of the relative width (level 95%) for *MinT* and *t-Rec* with  $T = 12$ . We report the results obtained with different values of  $T$  in Fig. B.11, Appendix B. The relative width of *MinT* is consistently  $< 1$ , in line with the theoretical analysis of *MinT* (Zambon et al., 2024a). On the other hand, the relative width of *t-Rec* is sometimes above 1, and it is positively correlated to the scaled incoherence of the base forecasts.

In Table 1, we report the geometric mean, over the simulations, of the relative width of the 80% and 95% PIs. The relative width of *MinT* depends on the ratio of the standard deviations of the reconciled and the

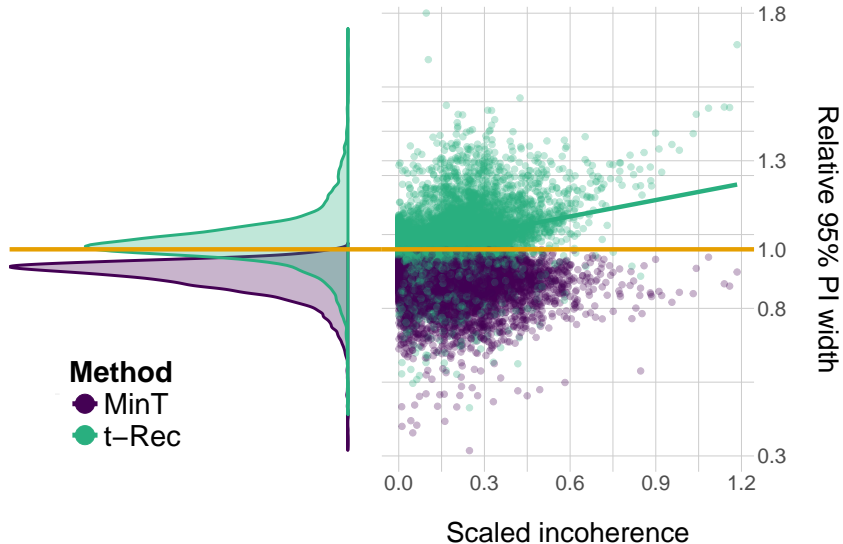


Figure 4: Left: distribution of the relative widths, i.e., reconciled PI width/base forecast PI width. We consider the 95% prediction intervals for the upper series for *MinT* (purple) and *t-Rec* (green), across 10 000 simulations with  $T=12$ . While *MinT* always narrows the prediction intervals, *t-Rec* can also widen them. Right: for each simulation, the relative widths of *MinT* and *t-Rec* are plotted against the scaled incoherence  $|\hat{a} - \hat{b}_1 - \hat{b}_2| / Q^{1/2}$ . Notably, *t-Rec* exhibits correlation, with interval widths expanding as incoherence grows.

base forecasts; it is thus the same at any confidence level. Instead, the relative width of *t-Rec* varies with the confidence level. Due to the heavier tails of the t-distribution compared to the Gaussian, the relative width of *t-Rec* is higher at the 95% level than at the 80%.

	Relative width			
	80%		95%	
	<i>MinT</i>	<i>t-Rec</i>	<i>MinT</i>	<i>t-Rec</i>
U	0.90	0.99	0.90	1.02
B1	0.95	1.01	0.95	1.05
B2	0.95	1.01	0.95	1.05

Table 1: Geometric average over 10 000 experiments of the relative widths with  $T = 12$ .

Finally, we measure the effect of accounting for the uncertainty on the covariance matrix  $\mathbf{W}$ . We compare *t-Rec* with *t-Rec-MAP*, i.e., *MinT* equipped with a covariance matrix corresponding to the mode of the Inverse-Wishart posterior distribution. Thus *t-Rec-MAP* adopt the maximum a posteriori point estimate of  $\mathbf{W}$ , while *t-Rec* accounts for the whole posterior distribution of  $\mathbf{W}$ . We run the simulations with increasing training lengths  $T$  (Fig. 5). For small values of  $T$ , the PIs of *t-Rec* are wider than the PIs of *t-Rec-MAP*, because of the uncertainty on  $\mathbf{W}$ . However the posterior uncertainty on  $\mathbf{W}$  decreases with  $T$  and eventually for large  $T$  the PIs of *t-Rec* and *t-Rec-MAP* become equivalent.

## 5. Experiments on real datasets

We compare *t-Rec* and *MinT* on three real-world datasets. The first is *Swiss tourism*, which we introduced for the first time; the other two are taken from previous papers and regard Australian tourism. Our code and the Swiss tourism dataset is available for reviewers in an anonymous GitHub <sup>1</sup>. We will release them in a public package after acceptance.

<sup>1</sup>Link to Anonymized GitHub

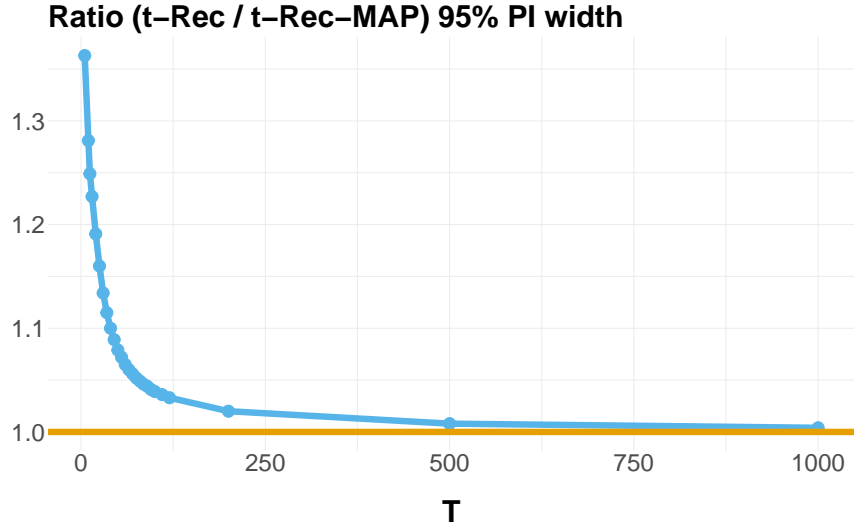


Figure 5: Geometric mean, computed over 10 000 independent experiments for each value of  $T$ , of the ratios between the 95% prediction interval widths of  $t$ -Rec and  $t$ -Rec-MAP. The average ratio converges to 1 as the training length grows.

*Swiss tourism.* Switzerland is divided in 26 cantons, listed in Table C.4, Appendix C. We consider monthly time series of overnight stays, downloaded from the website of the Swiss Federal Statistical Office <sup>2</sup>. The data are originally disaggregated by both canton and country of origin of the tourists. However, we restrict our analysis to the canton level, as further disaggregation yields time series with low counts and many zeros, for which the assumption of Gaussianity of the residuals is untenable. The resulting hierarchy consists of 26 bottom-level series (one for each canton) and one top-level series (Swiss total). Each time series goes from January 2005 to January 2025, i.e., 241 monthly observations.

*Australian tourism.* The other two datasets (*Australian Tourism-M* and *Australian Tourism-Q*) refer to Australian domestic overnight trips. We obtain the monthly dataset (*Australian Tourism-M*) from Rob J Hyndman’s website <sup>3</sup>. The bottom level includes 76 series representing Australian regions, which are then aggregated into 21 zones, 7 states, and the total. This dataset spans from January 1998 to December 2016, covering 228 time points. For more details, see Table 6 in Wickramasuriya et al. (2019).

Some regions are however composed by a single zone. In Wickramasuriya et al. (2019) they are in practice counted twice, both as region and as zone. We instead do not include zones composed by a single region; such regions are aggregated at the state level.

We take the quarterly data set *Australian Tourism-Q* from the `tsibble` R package (Wang, Cook & Hyndman, 2020). This is a two-level hierarchy, similar to the previous dataset but without the zone level. This dataset covers 20 years, from January 1998 to December 2017, for a total of 80 observations. The main features of all datasets are summarized in Table 2.

Dataset	Frequency	Levels	$n_b$	$n_u$	$n$	Length
Swiss Tourism	Monthly	1	26	1	27	240
Australian Tourism-M	Monthly	3	76	29	105	228
Australian Tourism-Q	Quarterly	2	76	8	84	80

Table 2: Summary of the datasets.

*Experimental setting.* We compute the base forecasts for each time series using `ets` from the `forecast` R package Hyndman & Khandakar (2008). We only consider models with additive noise, as our reconciliation

<sup>2</sup>Swiss tourism data

<sup>3</sup>[https://robjhyndman.com/data/TourismData\\_v3.csv](https://robjhyndman.com/data/TourismData_v3.csv)

approaches assumes a Gaussian predictive distribution. We perform reconciliation with both *t-Rec* and *MinT*.

We evaluate performance across various training lengths, using a rolling origin scheme for each. We use 100 rolling origins for the monthly datasets (*Swiss tourism and Australian Tourism-M*). For *Australian Tourism-Q*, which has fewer observations, we use between 30 and 65 rolling origins, depending on the training length.

*Evaluation metrics.* We assess the point forecasts through the Mean Squared Error (MSE), averaged over the rolling origins:

$$\text{MSE} = \frac{1}{R} \sum_{i=1}^R \|\tilde{\mathbf{y}}_i - \mathbf{y}_i\|_2^2,$$

where  $\|\cdot\|_2$  is the Euclidean distance,  $R$  is the number of rolling origins,  $\tilde{\mathbf{y}}_i \in \mathbb{R}^n$  is the vector of the point forecasts for the  $i$ -th rolling origin, and  $\mathbf{y}_i \in \mathbb{R}^n$  is the vector of the corresponding actual values. We report the relative MSE, i.e., the ratio between the MSE of the reconciled and the base forecasts:

$$\text{RelMSE} = \frac{\text{MSE}}{\text{MSE}_{base}}. \quad (17)$$

For each series  $j$ , with  $j = 1, \dots, n$ , we assess the predictive distribution using the Continuous Ranked Probability Score (CRPS) (Gneiting & Raftery, 2007):

$$\text{CRPS}_j = \frac{1}{R} \sum_{i=1}^R \int_{-\infty}^{+\infty} (F_{i,j}(x) - \mathbb{I}(x \geq y_{i,j}))^2 dx,$$

where  $F_{i,j}$  is the predictive CDF for the  $i$ -th rolling origin and series  $j$  and  $y_{i,j}$  is the corresponding actual value. We compute the CRPS for both the Gaussian and t-distributions in closed form using the `scoringRules` R package (Jordan, Krüger & Lerch, 2019). We score the prediction intervals of each series using the Mean Interval Score (MIS) (Gneiting & Raftery, 2007):

$$\text{MIS}_j = \frac{1}{R} \sum_{i=1}^R \left( (u_{i,j}^\alpha - l_{i,j}^\alpha) + \frac{2}{\alpha} [(l_{i,j}^\alpha - y_{i,j})\mathbb{I}(y_{i,j} < l_{i,j}^\alpha) + (y_{i,j} - u_{i,j}^\alpha)\mathbb{I}(y_{i,j} > u_{i,j}^\alpha)] \right),$$

where  $l_{i,j}^\alpha$  and  $u_{i,j}^\alpha$  are the lower and upper bounds of the  $\alpha$ -level prediction interval for the  $i$ -th rolling origin and series  $j$ , and  $y_{i,j}$  is the corresponding actual value. We consider the 80% and 95% prediction intervals. The CRPS and MIS are univariate scale-dependent scoring rules; following Girolimetto et al. (2024), we aggregate the  $n$  scores into a unique one by taking the geometric mean of the relative scores with respect to the base forecasts:

$$\text{RelCRPS} = \left( \prod_{j=1}^n \frac{\text{CRPS}_j}{\text{CRPS}_{j,base}} \right)^{\frac{1}{n}}, \quad (18)$$

and we do the same with the relative MIS scores for the 80% and 95% prediction intervals.

Finally, we check the statistical significance of the differences between methods. For each time series and score, we average the score over the rolling origins. For each score, we rank the models on each time series. We then use the Friedman test (Demšar, 2006) followed by the Nemenyi post hoc to detect which models have a mean rank which is significantly worse than the model with the best mean rank. This procedure controls for multiple comparisons and it is also called MCB (Multiple Comparison with the Best, Koning, Franses, Hibon & Stekler (2005)). We use the implementation of the `tsutils` R package (Kourentzes, 2023)

### 5.1. Swiss Tourism results

We consider training lengths from 30 (two and a half years) to 60 (five years); the results are shown in Fig. 6 as a function of the training length.

On the MSE, *t-Rec* and *MinT* perform similarly across all training lengths (top-left plot). However, *t-Rec* shows a clear improvement in the predictive distribution, according to both CRPS (top-right) and MIS (bottom). Since the CRPS averages the quantile loss across all quantiles (Hyndman & Athanasopoulos,

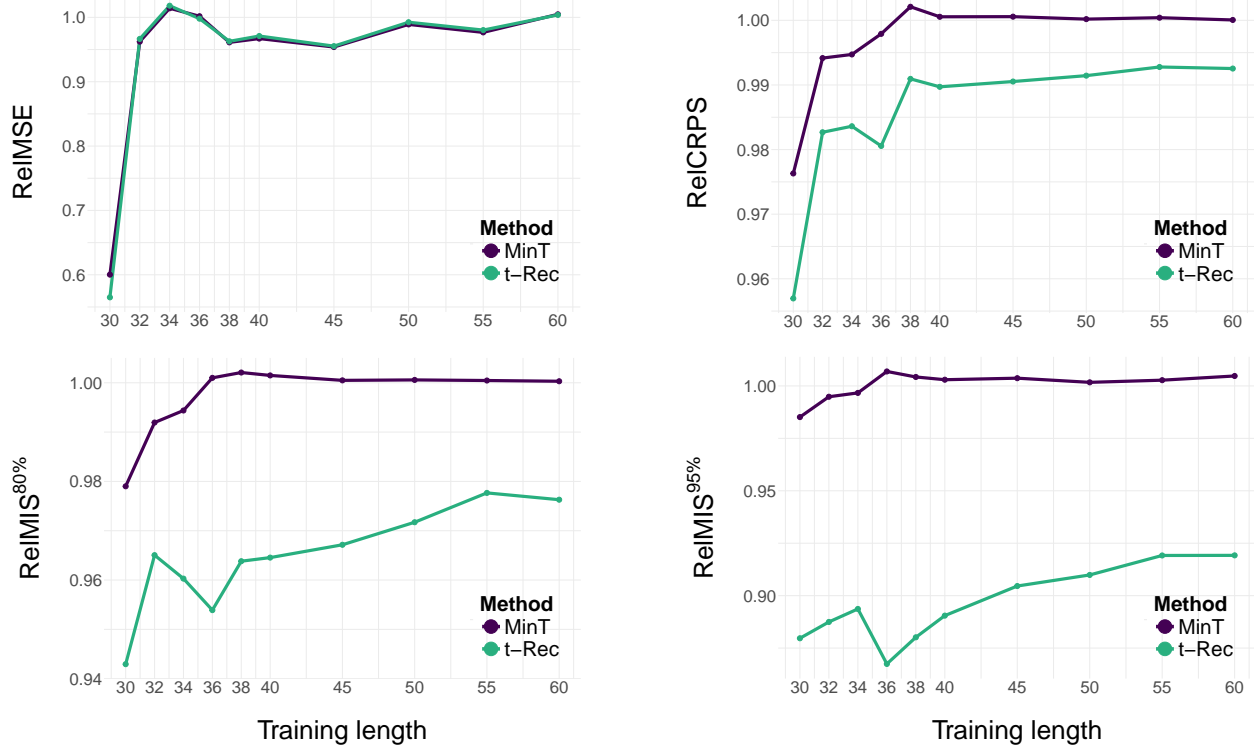


Figure 6: Results on the *Swiss Tourism* dataset for *MinT* (purple) and *t-Rec* (green), for the relative MSE (top-left), CRPS (top-right), and MIS (bottom-left: 80%, bottom-right: 95%). A relative score  $< 1$  means improvement over the base forecasts.

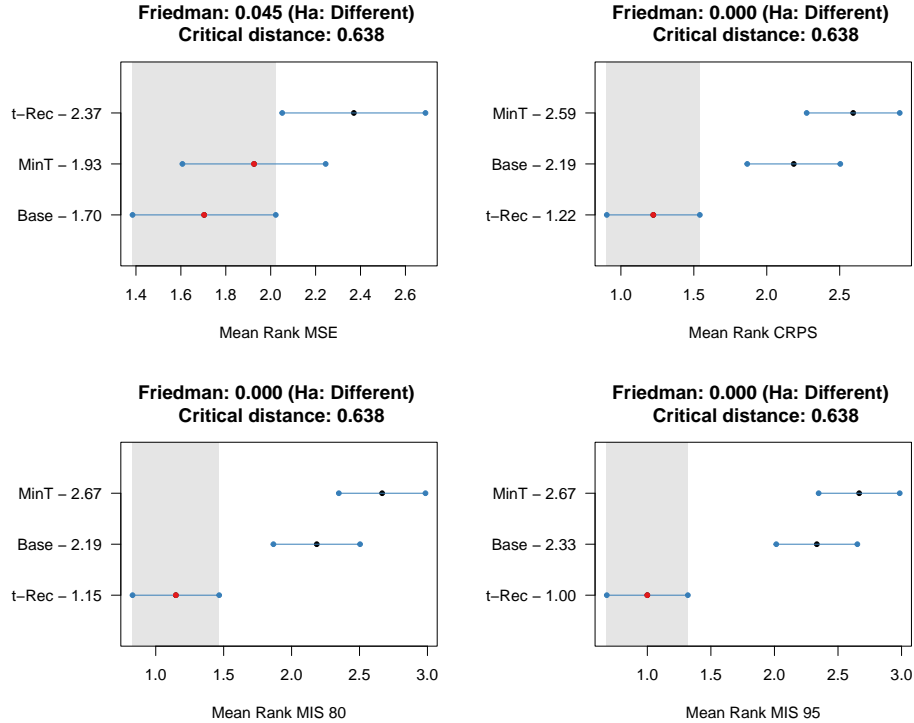


Figure 7: Friedman and post-hoc Nemenyi tests results for training length of 40 in the *Swiss Tourism* dataset for the MSE (top-left), CRPS (top-right), and MIS (bottom-left: 80%, bottom-right: 95%).

2021, Chap. 5.9) and  $t\text{-Rec}$  particularly enhances the tails of the predictive distributions, the improvement is more pronounced for the MIS, especially for the 95% intervals. Indeed, the  $t$ -distribution has polynomial tails, which allocate more probability mass to the extremes compared to the exponential tails of the Gaussian distribution used by  $MinT$ . Moreover,  $t\text{-Rec}$  provides better coverage than  $MinT$ ; the average coverage of the 95% prediction intervals is 88% for  $t\text{-Rec}$  and 83% for  $MinT$ . The improvement is consistent across all series, as shown in Fig. C.12, Appendix C.

Fig. 7 reports the results of the Friedman test with post-hoc for a training length of 40 observations. The titles report the p-value of the Friedman tests, the red dots represent the mean rank of the best method whose value is also reported on the y-axis label. Methods that are outside of the shaded areas perform significantly worse than the best method.

Fig. 8 reports the relative MIS for the 95% prediction intervals at the canton level for a training length of 40 observations. These results further confirm that  $t\text{-Rec}$  yields higher-scoring prediction intervals than  $MinT$ .

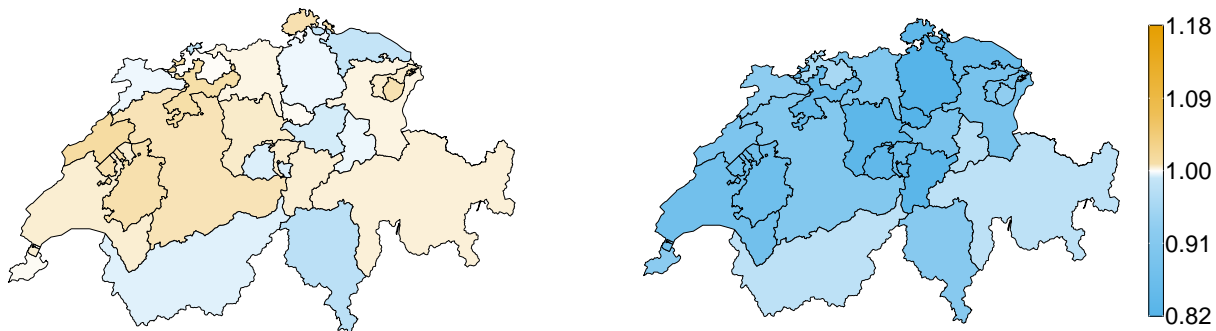


Figure 8: Relative  $MIS^{95\%}$  of  $MinT$  (left) and  $t\text{-Rec}$  (right) for each canton of the *Swiss Tourism* dataset (training length 40). Orange-colored cantons indicate worse performance compared to the base forecasts (ratio  $> 1$ ).  $t\text{-Rec}$  consistently improves  $MIS^{95\%}$  across all cantons and achieves greater absolute gains compared to  $MinT$ .

## 5.2. Australian Tourism results

We observe the same patterns also on *Australian tourism-M* and *Australian tourism-Q*. In terms of MSE,  $t\text{-Rec}$  and  $MinT$  perform similarly, indicating comparable point forecast accuracy. However,  $t\text{-Rec}$  yields better probabilistic forecasts, with a slight advantage in CRPS and substantial improvements in MIS, particularly at the 95% level, reflecting more reliable prediction intervals (Fig. 9).

We also compute the geometric mean of prediction interval widths and the arithmetic mean of coverage rates across the time series. We report the results for two different training lengths in Table 3. As for the *Swiss Tourism* dataset,  $t\text{-Rec}$  produces wider intervals than  $MinT$ , resulting in average coverage rates closer to the nominal levels (80% or 95%). The statistical analysis based on MCB confirms that  $t\text{-Rec}$  significantly improves the MIS score at both 80% and 95% levels compared to both  $MinT$  and the base forecasts.

		Australian Tourism - M				Australian Tourism - Q			
		Train 55		Train 110		Train 25		Train 40	
	Level	$MinT$	$t\text{-Rec}$	$MinT$	$t\text{-Rec}$	$MinT$	$t\text{-Rec}$	$MinT$	$t\text{-Rec}$
<b>PI Width</b>	80%	0.87	0.92	0.91	0.94	0.95	1.09	0.96	1.12
	95%	0.87	0.93	0.91	0.94	0.95	1.11	0.96	1.13
<b>Coverage</b>	80%	0.73	0.76	0.78	0.80	0.69	0.76	0.69	0.77
	95%	0.88	0.90	0.91	0.92	0.86	0.92	0.87	0.93

Table 3: Prediction interval (PI) width and coverage at the 80% and 95% confidence levels for the *Australian Tourism-M* and *Australian Tourism-Q* datasets. Results are reported for various training lengths.

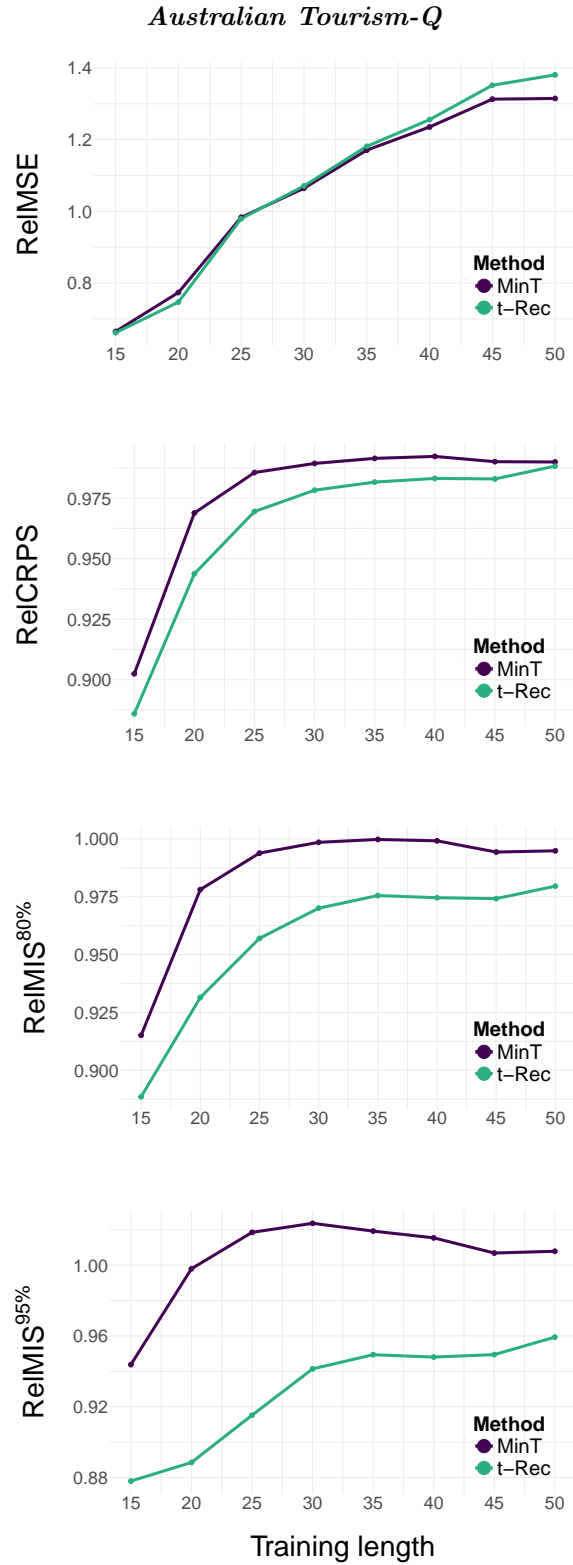
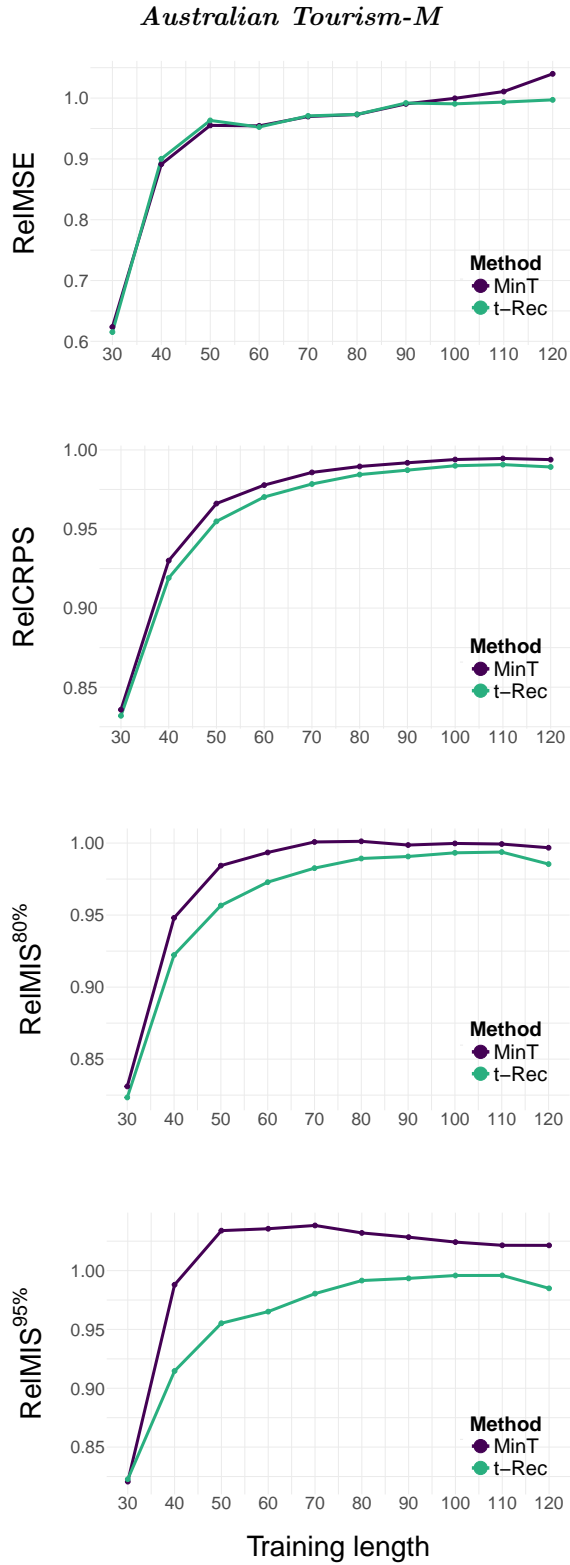


Figure 9: Results on the *Australian Tourism-M* (left column) and *Australian Tourism-Q* (right column) datasets for *MinT* (purple) and *t-Rec* (green). A relative score lower than 1 means improvement over the base forecasts.

### 5.3. Ablation study

To isolate the contributions of specific components of our method, we conduct an ablation study comparing  $t$ -Rec against three variants:

- $t$ -Rec-Diag: the prior scale matrix  $\Psi_0$  is specified as in  $t$ -Rec but restricted to be diagonal, ignoring prior correlations;
- $t$ -Rec-min\_ $\nu_0$ : the  $\nu_0$  parameter is fixed at its minimum admissible value ( $n + 2$ ), skipping the optimization procedure and making the prior weakly informative;
- $t$ -Rec-MAP (see Sect. 4.1): a maximum a posteriori point estimate is used for  $\mathbf{W}$ , instead of marginalizing over its posterior distribution.

We present the results for the *Swiss Tourism* dataset in Fig. 10. Additional experiments on the *Australian Tourism-M* and *Australian Tourism-Q* datasets yield similar results and are reported in Fig. C.13. Point forecast accuracy is largely equivalent across methods, with the exception of  $t$ -Rec-min\_ $\nu_0$ , which suffers from insufficient shrinkage due to the minimal value of  $\nu_0$ . However, significant differences emerge in probabilistic assessments, where  $t$ -Rec consistently achieves the best CRPS and MIS scores across different training lengths  $T$ . Specifically,  $t$ -Rec-MAP exhibits the poorest performance: since it uses a point estimate of the covariance matrix, it does not account for its uncertainty, yielding prediction intervals that are systematically too short. This highlights the fundamental role of the full Bayesian framework in incorporating covariance uncertainty. Furthermore, the suboptimal performance of  $t$ -Rec-min\_ $\nu_0$  validates the necessity of the optimization step for  $\nu_0$ . Finally, while the improvement of  $t$ -Rec over  $t$ -Rec-Diag is the smallest among the observed effects, it nonetheless confirms that prior information on the correlations among residuals from naive methods is informative and contributes to improved predictive performance.

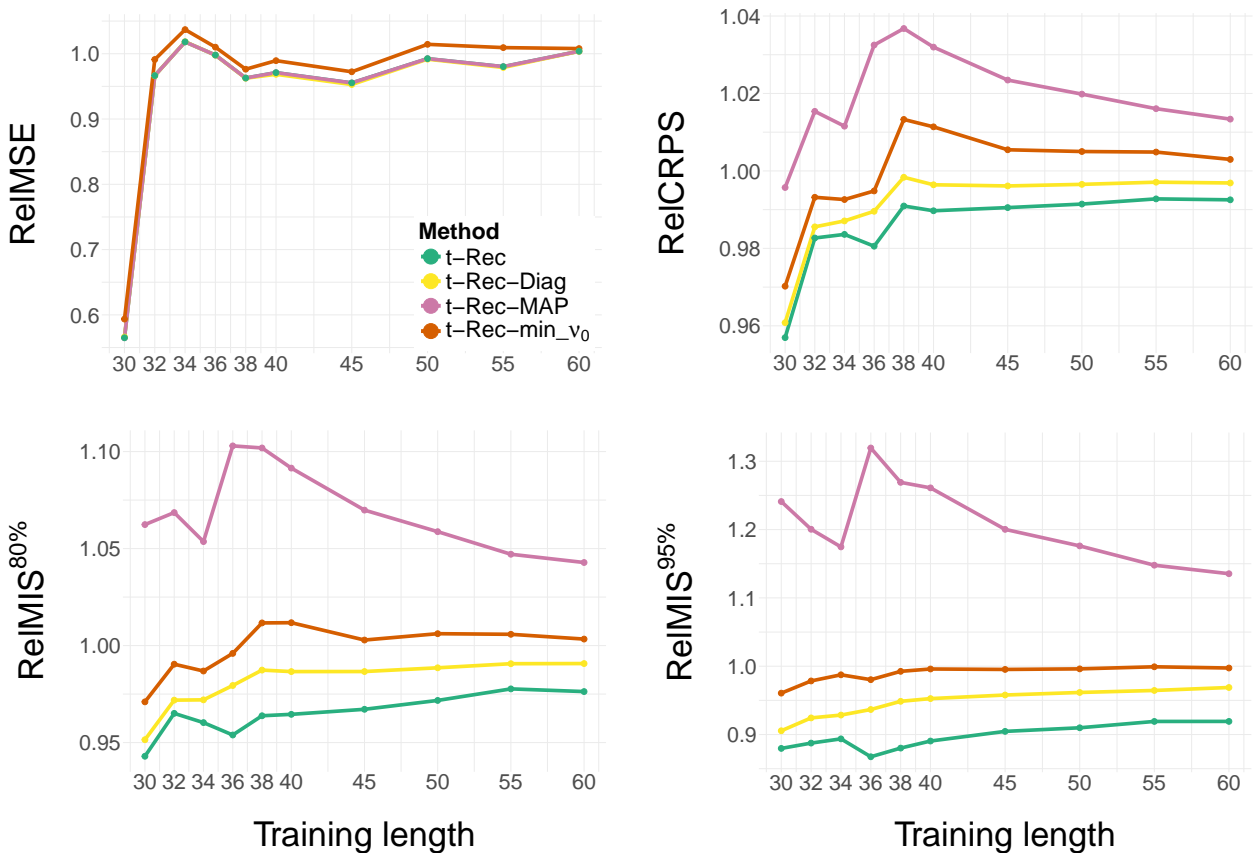


Figure 10: Results on *Swiss Tourism* dataset for  $t$ -Rec (green),  $t$ -Rec-Diag (yellow),  $t$ -Rec-MAP (pink) and  $t$ -Rec-min\_ $\nu_0$  (orange). A relative score lower than 1 means improvement over the base forecasts.

## 6. Conclusion

We propose *t-Rec*, a Bayesian method for probabilistic reconciliation that accounts for the uncertainty on the covariance matrix. Given our choices of prior and likelihood, we obtain in closed-form a multivariate-t reconciled predictive distribution. Empirical results show that *t-Rec* yields comparable point forecast accuracy to *MinT* but consistently outperforms it on the prediction intervals. Our results are robust across multiple datasets and various training set lengths.

Despite its robust performance, the effectiveness of *t-Rec* depends on the specification of the prior scale parameter  $\Psi_0$ . Our approach based on the residuals of the naive and seasonal naive methods may fail for complex time series with multiple seasonalities or strong covariate dependencies. In those cases, alternative specifications of  $\Psi_0$  might be necessary to maintain a well-specified prior. Moreover, we acknowledge the limitations of the Inverse-Wishart prior, particularly in high-dimensional settings (Gelman, 2006). Future work will explore more modern priors for the covariance matrix. Finally, our analysis focuses on the cross-sectional hierarchical setting; we leave for future studies the extension to temporal and cross-temporal hierarchies.

## References

- Athanasopoulos, G., Hyndman, R. J., Song, H., & Wu, D. C. (2011). The tourism forecasting competition. *International Journal of Forecasting*, *27*, 822–844.
- Bergmeir, C., Hyndman, R. J., & Koo, B. (2018). A note on the validity of cross-validation for evaluating autoregressive time series prediction. *Computational Statistics & Data Analysis*, *120*, 70–83.
- Carrara, C., Zambon, L., Azzimonti, D., & Corani, G. (2025). A novel shrinkage estimator of the covariance matrix for hierarchical time series. In E. di Bella, V. Gioia, C. Lagazio, & S. Zaccarin (Eds.), *Statistics for Innovation I* (pp. 140–145). Cham: Springer Nature Switzerland.
- Corani, G., Azzimonti, D., Augusto, J. P., & Zaffalon, M. (2020). Probabilistic Reconciliation of Hierarchical Forecast via Bayes’ Rule. In *Proc. European Conf. On Machine Learning and Knowledge Discovery in Database ECML/PKDD* (pp. 211–226). volume 3.
- Corani, G., Azzimonti, D., & Rubattu, N. (2024). Probabilistic reconciliation of count time series. *International Journal of Forecasting*, *40*, 457–469.
- Demšar, J. (2006). Statistical comparisons of classifiers over multiple data sets. *Journal of Machine learning research*, *7*, 1–30.
- Di Fonzo, T., & Girolimetto, D. (2024). Forecast combination-based forecast reconciliation: Insights and extensions. *International Journal of Forecasting*, *40*, 490–514.
- Ding, P. (2016). On the conditional distribution of the multivariate t distribution. *The American Statistician*, *70*, 293–295.
- Gelman, A. (2006). Prior distributions for variance parameters in hierarchical models (Comment on Article by Browne and Draper). *Bayesian Analysis*, *1*, 515–534.
- Gelman, A., Carlin, J., Stern, H., Dunson, D., Vehtari, A., & Rubin, D. (2013). *Bayesian Data Analysis (3rd ed.)*. Chapman and Hall/CRC.
- Girolimetto, D., Athanasopoulos, G., Di Fonzo, T., & Hyndman, R. J. (2024). Cross-temporal probabilistic forecast reconciliation: Methodological and practical issues. *International Journal of Forecasting*, *40*, 1134–1151.
- Girolimetto, D., & Di Fonzo, T. (2024). Point and probabilistic forecast reconciliation for general linearly constrained multiple time series. *Statistical Methods & Applications*, *33*, 581–607.
- Gneiting, T., & Raftery, A. E. (2007). Strictly proper scoring rules, prediction, and estimation. *Journal of the American statistical Association*, *102*, 359–378.

- Gupta, A. K., & Nagar, D. K. (2018). *Matrix variate distributions*. Chapman and Hall/CRC.
- Hyndman, R. J., Ahmed, R. A., Athanasopoulos, G., & Shang, H. L. (2011). Optimal combination forecasts for hierarchical time series. *Computational Statistics & Data Analysis*, *55*, 2579 – 2589.
- Hyndman, R. J., & Athanasopoulos, G. (2021). *Forecasting: principles and practice, 3rd edition*. OTexts. URL: [OTexts.com/fpp3](https://otexts.com/fpp3).
- Hyndman, R. J., & Khandakar, Y. (2008). Automatic time series forecasting: the forecast package for R. *Journal of statistical software*, *27*, 1–22.
- Johnson, S. G. (2008). *The NLOpt nonlinear-optimization package*. URL: <https://github.com/stevengj/nlopt>.
- Jordan, A., Krüger, F., & Lerch, S. (2019). Evaluating Probabilistic Forecasts with scoringRules. *Journal of Statistical Software*, *90*, 1–37.
- Koning, A. J., Franses, P. H., Hibon, M., & Stekler, H. (2005). The m3 competition: Statistical tests of the results. *International Journal of Forecasting*, *21*, 397–409. doi:10.1016/j.ijforecast.2004.10.003.
- Kotz, S., & Nadarajah, S. (2004). *Multivariate t-distributions and their applications*. Cambridge University Press.
- Kourentzes, N. (2023). *tsutils: Time Series Exploration, Modelling and Forecasting*. R package version 0.9.4.
- Panagiotelis, A., Athanasopoulos, G., Gamakumara, P., & Hyndman, R. J. (2021). Forecast reconciliation: A geometric view with new insights on bias correction. *International Journal of Forecasting*, *37*, 343–359.
- Panagiotelis, A., Gamakumara, P., Athanasopoulos, G., & Hyndman, R. J. (2023). Probabilistic forecast reconciliation: Properties, evaluation and score optimisation. *European Journal of Operational Research*, *306*, 693–706.
- Principato, G., Stoltz, G., Amara-Ouali, Y., Goude, Y., Hamrouche, B., & Poggi, J.-M. (2025). Conformal prediction for hierarchical data. URL: <https://arxiv.org/abs/2411.13479>. arXiv:2411.13479.
- Pritularga, K. F., Svetunkov, I., & Kourentzes, N. (2021). Stochastic coherency in forecast reconciliation. *International Journal of Production Economics*, *240*, 108221.
- Schäfer, J., & Strimmer, K. (2005). A shrinkage approach to large-scale covariance matrix estimation and implications for functional genomics. *Statistical applications in genetics and molecular biology*, *4*.
- Sherman, J., & Morrison, W. J. (1950). Adjustment of an inverse matrix corresponding to a change in one element of a given matrix. *The Annals of Mathematical Statistics*, *21*, 124–127.
- Svetunkov, I. (2023). *Forecasting and analytics with the augmented dynamic adaptive model (ADAM)*. CRC Press.
- Vehtari, A., Gelman, A., & Gabry, J. (2017). Practical Bayesian model evaluation using leave-one-out cross-validation and WAIC. *Statistics and computing*, *27*, 1413–1432.
- Wang, E., Cook, D., & Hyndman, R. J. (2020). A new tidy data structure to support exploration and modeling of temporal data. *Journal of Computational and Graphical Statistics*, *29*, 466–478.
- Wickramasuriya, S. L. (2017). *Optimal Forecasts for Hierarchical and Grouped Time Series*. Ph.D. thesis Monash University.
- Wickramasuriya, S. L. (2024). Probabilistic forecast reconciliation under the Gaussian framework. *Journal of Business & Economic Statistics*, *42*, 272–285.
- Wickramasuriya, S. L., Athanasopoulos, G., & Hyndman, R. J. (2019). Optimal forecast reconciliation for hierarchical and grouped time series through trace minimization. *Journal of the American Statistical Association*, *114*, 804–819.

Zambon, L., Agosto, A., Giudici, P., & Corani, G. (2024a). Properties of the reconciled distributions for Gaussian and count forecasts. *International Journal of Forecasting*, *40*, 1438–1448.

Zambon, L., Azzimonti, D., & Corani, G. (2024b). Efficient probabilistic reconciliation of forecasts for real-valued and count time series. *Statistics and Computing*, *34*, 21.

## Appendix A. Reconciliation via conditioning of multivariate $\mathbf{t}$

Similarly to the Gaussian case (Zambon et al., 2024a), if the joint base forecast distribution is a multivariate  $\mathbf{t}$ , then the reconciled distribution and the parameters can be computed in closed-form. Theorem 1 is proved by applying the following result to Eq. (9) with  $\widehat{\Psi} = \frac{1}{\nu' - n + 1} \Psi'$  and  $\widehat{\nu} = \nu' - n + 1$ .

**Proposition 1.** *Let  $\mathbf{A} \in \mathbb{R}^{(n-n_b) \times n_b}$  be the aggregation matrix of a hierarchy with  $n$  time series, and let the joint forecast distribution be a multivariate  $\mathbf{t}$ :  $\widehat{\mathbf{Y}} \sim \text{mt}(\widehat{\mathbf{y}}, \widehat{\Psi}, \widehat{\nu}) = \text{mt}\left(\begin{bmatrix} \widehat{\mathbf{u}} \\ \widehat{\mathbf{b}} \end{bmatrix}, \begin{bmatrix} \Psi'_{UB} & \Psi'_{UB} \\ \Psi'_{BU} & \Psi'_{BU} \end{bmatrix}, \widehat{\nu}\right)$ . Then, the reconciled distribution via conditioning of the  $n_b$  bottom series is still a multivariate  $\mathbf{t}$ :*

$$\widetilde{\mathbf{B}} \sim \text{mt}(\widetilde{\mathbf{b}}, \widetilde{\Sigma}_B, \widetilde{\nu}), \quad (\text{A.1})$$

where

$$\widetilde{\mathbf{b}} = \widehat{\mathbf{b}} + \left( \widehat{\Psi}_{UB}^T - \widehat{\Psi}_B \mathbf{A}^T \right) \mathbf{Q}^{-1} (\mathbf{A} \widehat{\mathbf{b}} - \widehat{\mathbf{u}}), \quad (\text{A.2})$$

$$\widetilde{\Sigma}_B = C \left[ \widehat{\Psi}_B - \left( \widehat{\Psi}_{UB}^T - \widehat{\Psi}_B \mathbf{A}^T \right) \mathbf{Q}^{-1} \left( \widehat{\Psi}_{UB}^T - \widehat{\Psi}_B \mathbf{A}^T \right)^T \right], \quad (\text{A.3})$$

$$\widetilde{\nu} = \widehat{\nu} + n - n_b, \quad (\text{A.4})$$

and

$$C = \frac{\widehat{\nu} + (\mathbf{A} \widehat{\mathbf{b}} - \widehat{\mathbf{u}})^T \mathbf{Q}^{-1} (\mathbf{A} \widehat{\mathbf{b}} - \widehat{\mathbf{u}})}{\widehat{\nu} + (n - n_b)},$$

$$\mathbf{Q} = \widehat{\Psi}_U - \widehat{\Psi}_{UB} \mathbf{A}^T - \mathbf{A} \widehat{\Psi}_{UB}^T + \mathbf{A} \widehat{\Psi}_B \mathbf{A}^T. \quad (\text{A.5})$$

To prove Proposition 1, we first state two technical lemmas about key properties of the multivariate  $\mathbf{t}$  distribution. We refer to Kotz & Nadarajah (2004) for the proof of Lemma 1 and to Ding (2016) for the proof of Lemma 2.

**Lemma 1.** *Let  $\mathbf{X}$  be a  $n$ -dimensional random vector distributed as a multivariate  $\mathbf{t}$ :*

$$\mathbf{X} \sim \text{mt}(\boldsymbol{\mu}, \Sigma, \nu),$$

and let  $\mathbf{V} \in \mathbb{R}^{n \times n}$  be full-rank. Then, the random vector  $\mathbf{V}\mathbf{X}$  is distributed as a multivariate  $\mathbf{t}$ :

$$\mathbf{V}\mathbf{X} \sim \text{mt}(\mathbf{V}\boldsymbol{\mu}, \mathbf{V}\Sigma\mathbf{V}^T, \nu).$$

**Lemma 2.** *Let  $\mathbf{X} = \begin{bmatrix} \mathbf{X}_1 \\ \mathbf{X}_2 \end{bmatrix} \sim \text{mt}\left(\begin{bmatrix} \boldsymbol{\mu}_1 \\ \boldsymbol{\mu}_2 \end{bmatrix}, \begin{bmatrix} \Sigma_{11} & \Sigma_{12} \\ \Sigma_{21} & \Sigma_{22} \end{bmatrix}, \nu\right)$ , where  $\mathbf{X} \in \mathbb{R}^n$ ,  $\mathbf{X}_1 \in \mathbb{R}^{n_1}$ ,  $\mathbf{X}_2 \in \mathbb{R}^{n_2}$  and  $n_1 + n_2 = n$ . Then, the conditional distribution of  $\mathbf{X}_1$  given  $\mathbf{X}_2$  is still a multivariate  $\mathbf{t}$ :*

$$\mathbf{X}_1 | \mathbf{X}_2 \sim \text{mt}(\boldsymbol{\mu}_{1|2}, \Sigma_{1|2}, \nu_{1|2}), \quad (\text{A.6})$$

where

$$\boldsymbol{\mu}_{1|2} = \boldsymbol{\mu}_1 + \Sigma_{12} \Sigma_{22}^{-1} (\mathbf{x}_2 - \boldsymbol{\mu}_2), \quad (\text{A.7})$$

$$\Sigma_{1|2} = \frac{\nu + (\mathbf{x}_2 - \boldsymbol{\mu}_2)^T \Sigma_{22}^{-1} (\mathbf{x}_2 - \boldsymbol{\mu}_2)}{\nu + n_2} [\Sigma_{11} - \Sigma_{12} \Sigma_{22}^{-1} \Sigma_{21}], \quad (\text{A.8})$$

$$\nu_{1|2} = \nu + n_2. \quad (\text{A.9})$$

*Proof of Proposition 1.* Let us define  $\mathbf{T} \in \mathbb{R}^{n \times n}$  as

$$\mathbf{T} = \begin{bmatrix} \mathbf{0} & \mathbf{I}_{n_b} \\ \mathbf{I}_{n-n_b} & -\mathbf{A} \end{bmatrix},$$

and let  $\mathbf{Z} := \mathbf{T}\hat{\mathbf{Y}}$ . Since  $\mathbf{T}$  is full-rank, from Lemma 1,  $\mathbf{Z}$  is a multivariate t:

$$\mathbf{Z} \sim \text{mt} \left( \mathbf{T}\hat{\mathbf{y}}, \mathbf{T}\hat{\Psi}\mathbf{T}^T, \hat{\nu} \right), \quad (\text{A.10})$$

where

$$\begin{aligned} \mathbf{T}\hat{\mathbf{y}} &= \begin{bmatrix} \hat{\mathbf{b}} \\ \hat{\mathbf{u}} - \mathbf{A}\hat{\mathbf{b}} \end{bmatrix}, \\ \mathbf{T}\hat{\Psi}\mathbf{T}^T &= \begin{bmatrix} \hat{\Psi}_B & \hat{\Psi}_{UB}^T - \hat{\Psi}_B\mathbf{A}^T \\ \hat{\Psi}_{UB} - \mathbf{A}\hat{\Psi}_B & \mathbf{Q} \end{bmatrix}, \end{aligned} \quad (\text{A.11})$$

and  $\mathbf{Q} = \hat{\Psi}_U - \hat{\Psi}_{UB}\mathbf{A}^T - \mathbf{A}\hat{\Psi}_{UB}^T + \mathbf{A}\hat{\Psi}_B\mathbf{A}^T$ . Since

$$\mathbf{Z} = \begin{bmatrix} \hat{\mathbf{B}} \\ \hat{\mathbf{U}} - \mathbf{A}\hat{\mathbf{B}} \end{bmatrix} =: \begin{bmatrix} \mathbf{Z}_1 \\ \mathbf{Z}_2 \end{bmatrix},$$

the reconciled bottom distribution, specified by Eq. (3), is given by the conditional distribution of  $\mathbf{Z}_1$  given  $\mathbf{Z}_2 = 0$ . From Lemma 2, we have that

$$\mathbf{Z}_1 | \mathbf{Z}_2 = 0 \sim \text{mt} \left( \boldsymbol{\mu}_{1|2}, \boldsymbol{\Sigma}_{1|2}, \nu_{1|2} \right),$$

where

$$\begin{aligned} \boldsymbol{\mu}_{1|2} &= \hat{\mathbf{b}} + \left( \hat{\Psi}_{UB}^T - \hat{\Psi}_B\mathbf{A}^T \right) \mathbf{Q}^{-1} (\mathbf{A}\hat{\mathbf{b}} - \hat{\mathbf{u}}) = \tilde{\mathbf{b}}, \\ \nu_{1|2} &= \hat{\nu} + (n - n_b) = \tilde{\nu}, \\ \boldsymbol{\Sigma}_{1|2} &= \frac{\hat{\nu} + (\mathbf{A}\hat{\mathbf{b}} - \hat{\mathbf{u}})^T \mathbf{Q}^{-1} (\mathbf{A}\hat{\mathbf{b}} - \hat{\mathbf{u}})}{\hat{\nu} + (n - n_b)} \left[ \hat{\Psi}_B - \left( \hat{\Psi}_{UB}^T - \hat{\Psi}_B\mathbf{A}^T \right) \mathbf{Q}^{-1} \left( \hat{\Psi}_{UB}^T - \hat{\Psi}_B\mathbf{A}^T \right)^T \right] \\ &= C \left[ \hat{\Psi}_B - \left( \hat{\Psi}_{UB}^T - \hat{\Psi}_B\mathbf{A}^T \right) \mathbf{Q}^{-1} \left( \hat{\Psi}_{UB}^T - \hat{\Psi}_B\mathbf{A}^T \right)^T \right] = \tilde{\boldsymbol{\Sigma}}_B. \end{aligned}$$

□

#### Appendix A.1. Reconciliation of a minimal hierarchy

We explicitly write the expression of the reconciled t-distribution on a minimal hierarchy with 1 upper and 2 bottom series (Fig. 3) using Theorem 1. The reconciled bottom and upper distribution are multivariate t and univariate t:

$$\tilde{\mathbf{B}} \sim \text{mt} \left( \tilde{\mathbf{b}}, \tilde{\boldsymbol{\Sigma}}_B, \tilde{\nu} \right), \quad \tilde{U} \sim \text{t} \left( \tilde{u}, \tilde{\sigma}_u, \tilde{\nu} \right), \quad (\text{A.12})$$

where

$$\begin{aligned} \tilde{\nu} &= \nu' - 1, \\ \tilde{\mathbf{b}} &= \begin{bmatrix} \left( 1 - \frac{g_1}{Q} \right) \hat{b}_1 + \frac{g_1}{Q} \left( \hat{u} - \hat{b}_2 \right) \\ \left( 1 - \frac{g_2}{Q} \right) \hat{b}_2 + \frac{g_2}{Q} \left( \hat{u} - \hat{b}_1 \right) \end{bmatrix}, \quad \tilde{u} = \left( 1 - \frac{g_u}{Q} \right) \hat{u} + \frac{g_u}{Q} \left( \hat{b}_1 + \hat{b}_2 \right), \end{aligned} \quad (\text{A.13})$$

$$\tilde{\boldsymbol{\Sigma}}_B = C \begin{bmatrix} \Psi'_1 - \frac{g_1^2}{Q} & \Psi'_{1,2} - \frac{g_1 g_2}{Q} \\ \Psi'_{1,2} - \frac{g_1 g_2}{Q} & \Psi'_2 - \frac{g_2^2}{Q} \end{bmatrix}, \quad \tilde{\sigma}_u^2 = C \left( \Psi'_u - \frac{g_u^2}{Q} \right), \quad (\text{A.14})$$

and

$$\begin{aligned} C &= \frac{1}{\tilde{\nu}} \left( 1 + \frac{(\hat{b}_1 + \hat{b}_2 - \hat{u})^2}{Q} \right), & Q &= g_1 + g_2 + g_u, \\ g_1 &= (\Psi'_1 + \Psi'_{1,2}) - \Psi'_{u,1}, & \Psi' &= \begin{bmatrix} \Psi'_u & \Psi'_{u,1} & \Psi'_{u,2} \\ \Psi'_{u,1} & \Psi'_1 & \Psi'_{1,2} \\ \Psi'_{u,2} & \Psi'_{1,2} & \Psi'_2 \end{bmatrix}. \\ g_2 &= (\Psi'_2 + \Psi'_{1,2}) - \Psi'_{u,2}, \\ g_u &= \Psi'_u - \Psi'_{u,1} - \Psi'_{u,2}, \end{aligned}$$

## Appendix B. Additional details and results for the simulations

*Simulation setup.* For the experiments in Sect. 4, we adopt a simulation framework similar to that described in Sect. 3.4 of Wickramasuriya et al. (2019). We consider the minimal hierarchy of Fig. 3. The length of the time series is set to 12. The bottom-level time series are simulated using a basic structural time series model defined as:

$$\mathbf{b}_t = \boldsymbol{\mu}_t + \boldsymbol{\gamma}_t + \boldsymbol{\eta}_t,$$

where  $\boldsymbol{\mu}_t$  is the trend component,  $\boldsymbol{\gamma}_t$  is the seasonal component, and  $\boldsymbol{\eta}_t$  is the error component. The trend component evolves according to a local linear trend model:

$$\begin{aligned} \boldsymbol{\mu}_t &= \boldsymbol{\mu}_{t-1} + \boldsymbol{\nu}_t + \boldsymbol{\varepsilon}_t, & \boldsymbol{\varepsilon}_t &\sim \mathcal{N}(0, 2I_2), \\ \boldsymbol{\nu}_t &= \boldsymbol{\nu}_{t-1} + \boldsymbol{\zeta}_t, & \boldsymbol{\zeta}_t &\sim \mathcal{N}(0, 0.007I_2), \end{aligned}$$

where  $\boldsymbol{\varepsilon}_t$ ,  $\boldsymbol{\zeta}_t$ , and  $\boldsymbol{\omega}_t$  are mutually independent and also independent over time. The seasonal component is defined by:

$$\boldsymbol{\gamma}_t = - \sum_{i=1}^{s-1} \boldsymbol{\gamma}_{t-i} + \boldsymbol{\omega}_t, \quad \boldsymbol{\omega}_t \sim \mathcal{N}(0, 7I_2),$$

with the number of seasons per year set to  $s = 4$  to reflect quarterly data. The initial states  $\boldsymbol{\mu}_0$ ,  $\boldsymbol{\nu}_0$ ,  $\boldsymbol{\gamma}_0$ ,  $\boldsymbol{\gamma}_1$ , and  $\boldsymbol{\gamma}_2$  are independently drawn from a multivariate normal distribution with mean zero and identity covariance matrix. The error component  $\boldsymbol{\eta}_t$  for each series is generated from an ARIMA(1, 0, 1) model with  $\phi_1 = 0.3$  and  $\theta_1 = 0.5$ ; we use  $\begin{bmatrix} 5 & 3 \\ 3 & 4 \end{bmatrix}$  as contemporaneous error covariance matrix, the same of series AA and AB in Wickramasuriya et al. (2019). Finally, the upper series is obtained by summing the bottom series.

*Simulation study for different training lengths.* In Fig. B.11, we show the distribution of the relative widths (i.e., reconciled PI width/base forecast PI width) of  $t$ -Rec and  $MinT$  for different values of  $T$ .

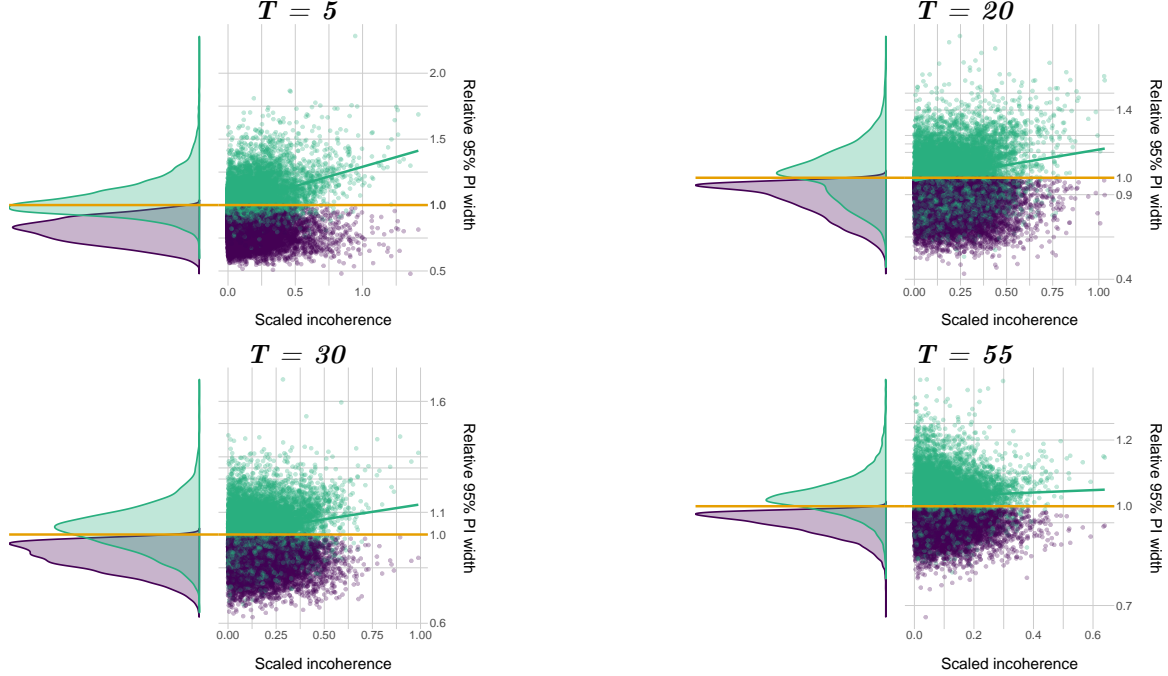


Figure B.11: Results of the simulations for different values of the training length  $T$ . In each plot: Left: distribution of the relative widths of the 95% PIs of the upper series for  $MinT$  (purple) and  $t$ -Rec (green), across 10 000 simulations. Right: for each simulation, the relative widths of  $MinT$  and  $t$ -Rec are plotted against the scaled incoherence  $|\hat{u} - \hat{b}_1 - \hat{b}_2| / Q^{1/2}$ . Notably, for  $t$ -Rec the dependence between the relative PI width and the scaled incoherence diminishes as  $T$  grows. This happens because, as  $T$  becomes large, the uncertainty on  $\mathbf{W}$  decreases and the predictive  $t$  distribution converges to a Gaussian. Since, in the Gaussian case, incoherence does not affect interval widths, the influence of the incoherence progressively vanishes.

## Appendix C. Additional results on real datasets

Abbr.	Canton	Abbr.	Canton	Abbr.	Canton
AG	Aargau	NW	Nidwalden	AI	Appenzell Innerrhoden
OW	Obwalden	AR	Appenzell Ausserrhoden	SG	St. Gallen
BE	Bern	SH	Schaffhausen	SO	Solothurn
BL	Basel-Landschaft	BS	Basel-Stadt	FR	Fribourg
GE	Geneva	GL	Glarus	GR	Graubünden
JU	Jura	LU	Lucerne	NE	Neuchâtel
SZ	Schwyz	TG	Thurgau	TI	Ticino
UR	Uri	VD	Vaud	VS	Valais
ZG	Zug	ZH	Zurich		

Table C.4: List of the 26 Swiss cantons.

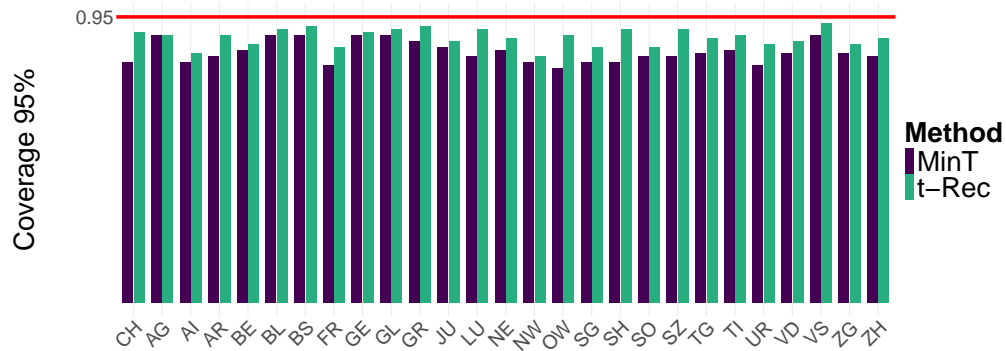


Figure C.12: Coverage of the 95% prediction intervals across 100 rolling origins (training length = 40) on the *Swiss Tourism* dataset. For each series, *t-Rec* achieves coverage closer to the target (red line) than *MinT*.

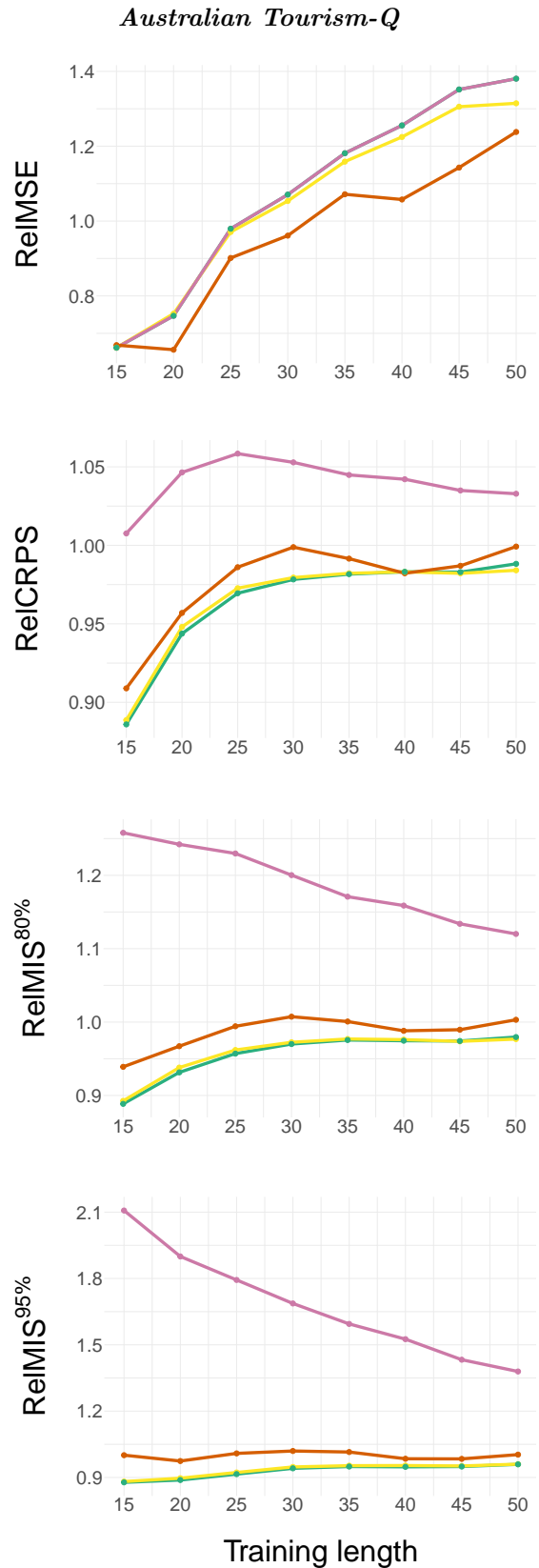
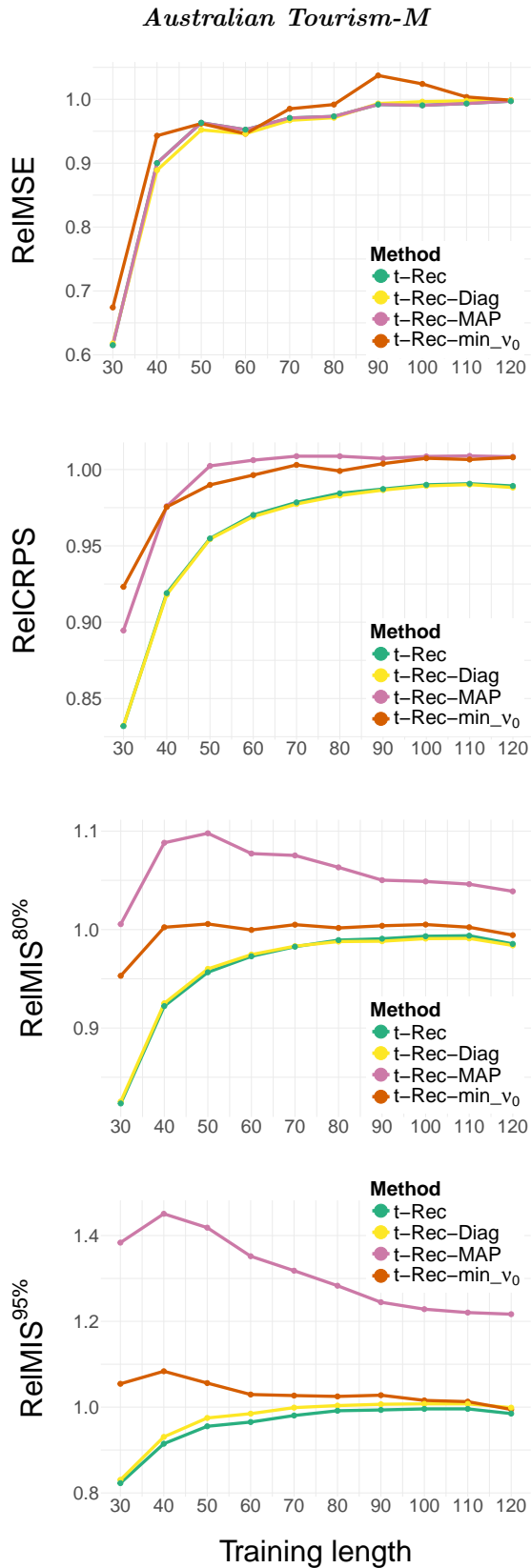


Figure C.13: Results on the *Australian Tourism-M* (left column) and *Australian Tourism-Q* (right column) datasets for *t-Rec* (green), *t-Rec-Diag* (yellow), *t-Rec-MAP* (pink) and *t-Rec-min\_v0* (orange). A relative score lower than 1 means improvement over the base forecasts.